Acid dissociation mechanisms of Si(OH)(4) and Al(H2O)(6)(3+) in aqueous solution

Liu, X.; Lu, X.; Meijer, E.J.; Wang, R.; Zhou, H.

DOI
10.1016/j.gca.2009.10.032

Publication date
2010

Document Version
Final published version

Published in
Geochimica et Cosmochimica Acta

Available online at www.sciencedirect.com
ScienceDirect
Geochimica et Cosmochimica Acta 74 (2010) 510–516
Geochimica et Cosmochimica Acta
www.elsevier.com/locate/gca

Acid dissociation mechanisms of $Si(OH)_4$ and $Al(H_2O)_6^{3+}$ in aqueous solution

Xiandong Liu [a,*], Xiancai Lu [a], Evert Jan Meijer [b], Rucheng Wang [a], Huiqun Zhou [a]

[a] State Key Laboratory for Mineral Deposit Research, School of Earth Sciences and Engineering, Nanjing University, Nanjing 210093, Hankou Road 22, PR China

[b] Van't Hoff Institute for Molecular Sciences and Amsterdam Center for Multiscale Modeling, University of Amsterdam, Nieuwe Achtergracht 166, 1018 WV Amsterdam, The Netherlands

Received 3 August 2009; accepted in revised form 15 October 2009; available online 27 October 2009

Abstract

Silicic acid and the hexa-aqua of Al^{3+} are fundamental model aqueous species of chemical importance in nature. In order to investigate their hydroxyl dissociation mechanisms, Car–Parrinello molecular dynamics (CPMD) simulations were carried out, which allow treating the solutes and solvents on the same footing. The method of constraint was employed to trigger the reactions by taking coordination number as the reaction coordinate and the thermodynamic integration was used to obtain the free-energy profiles. The approximate transition states were located and the reactant and product states were also characterized. The free-energy changes of dissociation are found about 15.0 kcal/mol and 7.7 kcal/mol for silicic acid and Al-aqua, respectively. From the simulation results, the first p*K*as were calculated by using two approaches, which are based on the pristine thermodynamic relation and the RDF (radial distribution function)-free energy relation, respectively. Because of more uncertainties involved in the RDF way, it is suggested that the pristine way should be favored, which shows an error margin of 1 p*K*a unit. This study provides an encouraging basis for applying the present methodology to predict acidity constants of those groups that are difficult to measure experimentally.

1. INTRODUCTION

Silicon and aluminium are respectively the second and the third most abundant elements on the earth. Understanding their aqueous chemistry is critical for geochemistry, environmental sciences and material syntheses (Iler, 1979; Sigel and Sigel, 1988; Yokel, 2004). Silicic acid and the hexa-aqua of Al^{3+} are their basic forms in water and according to hydroxyl dissociation and dehydration reactions, they can evolve to a broad spectrum of species in aqueous solutions, for example, $SiO(OH)_3^-$ and $SiO_2(OH)_2^{2-}$; $Al(H_2O)_5OH^{2+}$, $Al(H_2O)_4(OH)_2^+$ and $Al(OH)_4^-$ (StÖber, 1967; Martin, 1988, 1991). Furthermore, these species can form larger polynuclear clusters through condensation reactions, which eventually lead to the crystal growths, e.g. Al/Si containing (hydr)oxides, zeolites and clay minerals (Casey and Rustad, 2007; Casey et al., 2009; Trinh et al., 2009). In all of these processes, the dissociations of the coordinated hydroxyls and waters are key reaction steps and therefore, it is obvious that the relevant acidity constants and dissociation mechanisms are central for understanding their geochemical properties (Casey et al., 2009).

In the previous studies, first-principles techniques have been applied to investigate the dissociations of hydroxyls and water of the small Al- and Si- containing clusters. For example, Rustad et al. (2000a) found a correlation between the calculated gas-phase p*K*as and the measured aqueous phase values of silicic acid; Bickmore et al. (2004, 2006) have proposed a bond–valence approach to calculate acidity constants and applied it to a broad spectrum of species. In the studies of Kubicki (2001) and Sefcik and Goddard (2001), they correlated the deprotonation

* Corresponding author. Tel.: +86 25 83594664; fax: +86 25 83686016.
E-mail address: xiandongliu@gmail.com (X. Liu).

0016-7037/$ - see front matter © 2009 Elsevier Ltd. All rights reserved.
doi:10.1016/j.gca.2009.10.032

energies with the measured p*K*as. In those calculations, the solvent effects were simplified by inserting several water molecules around or with empirical continuum models. But actually, the products of those approaches are still far from the real nature of the reactive events in condensed phases. In condensed phase reactions, the dynamical fluctuations form the basis of entropy component of free energies (Sprik, 1998). However, in the traditional quantum chemical ways, almost all analyses are based on the static calculations, e.g. geometry optimization. Therefore the results are actually obtained under absolute zero and thus the entropy contribution is hard to include. Furthermore, in the reactions involving proton transfer, the solvents effects are more significant because the solvent (e.g. water) can directly participate in the reactions as reactant or catalyst (van Erp and Meijer, 2004; Marx, 2006). These factors make it necessary to treat the explicitly solvated systems under a finite temperature and by using full quantum mechanical techniques.

In this study, we employ first-principles molecular dynamics technique to investigate the dissociation mechanisms of $Si(OH)_4$ and $Al(H_2O)_6^{3+}$. With Car–Parrinello molecular dynamics (Car and Parrinello, 1985), the solutes and solvents are simulated on the same footing. The dissociation reaction is an activated process, i.e. it is far beyond the timescale accessible to present-day CPMD simulation (i.e. tens of picoseconds). We therefore enforce the reactive event by using the method of constraints (Carter et al., 1989; Sprik and Ciccotti, 1998), and calculate the free-energy profile by thermodynamic integration of the average constraint force and derive the acidity constants.

Another goal of this study is to test the methodology of p*K*a prediction. If the technique can be calibrated on these known small systems, it should be transferable to predicting the acidities of more complex systems of (geo)chemical importance, which are usually difficult to measure experimentally. For example, hydroxyls and chemically-adsorbed water widely distribute on the edge surfaces of clay minerals and (hydro)oxides (e.g. Si, Al, Mn, Fe-containing), which are highly chemically reactive and play active roles in many interfacial reactions (Rustad et al., 1999, 2000b, 2001; Bickmore et al., 2003; Churakov, 2006, 2007; Liu et al., 2008; Casey et al., 2009). For these systems, the broken surfaces are complicated by themselves and the electrostatics of the substrates spread into the solution phases, and therefore, the first-principle MD simulation seems the only possible way to tackle the dissociation mechanisms of the surface groups.

2. METHODOLOGY

2.1. Car–Parrinello MD

The simulation cell is a periodically repeated cubic box of side length 10.5 Å. The $Si(OH)_4$ and Al-aqua systems contain 34 and 38 water molecules, respectively, which reproduce the density of water under ambient condition. The electronic structures are calculated in the framework of density functional theory and the exchange-correlation is described by BLYP functional (Becke, 1988; Lee et al., 1988), which has been proven able to accurately describe the behaviors of water and proton (e.g. Laasonen et al., 1993; Marx et al., 1999). The norm-conserving Martins–Troullier pseudopotentials (Troullier and Martins, 1991) are used to describe the interaction of the valence electrons and the core states and the Kleinman–Bylander scheme (Kleinman and Bylander, 1982) is applied. The orbitals are expanded in plane wave basis sets with a kinetic energy cutoff of up to 70 Ry. For the $Al(H_2O)_6^{3+}$ system, a neutralizing background charge is added.

The molecular dynamics simulations are performed by using the CPMD package (CPMD version 3.11). The hydrogen is assigned a mass of deuterium. The fictitious electronic mass is set to 1200 au and the equation of motion is integrated with a time step of 0.168 fs, which maintains the adiabatic conditions. The temperature is controlled at 300 K with the Nosé–Hoover thermostat. For each constrained simulation, MD is carried out with the reaction coordinate fixed at the desired value. Each unconstrained/constrained MD trajectory includes a production step of 6 ps and a prior equilibration run lasting 3 ps. The statistics are collected every 6 steps for all simulations.

2.2. Method of constraint

The reaction event is enforced by the method of constraint and the relative free energies (ΔF) are obtained by integrating the averaged force (f) along the reaction coordinates via the thermodynamic integration relation,

$$\Delta F(Q) = -\int_{Q_0}^{Q} dQ' f(Q') \tag{1}$$

The reaction coordinate Q is some geometric parameter which represents the progress of the reaction path. It is an analytical function of the cartesian coordinate ($\mathbf{r}^N$), for example, bond-length, bond angle, torsion angle and coordination number.

For the distance constraint, it has been shown that the averaged force equals the Lagrange multiplier (λ) and for more general types, the force has the following form (Sprik and Ciccotti, 1998),

$$f(Q') = \frac{\langle Z^{-1/2}[\lambda - k_B T G]\rangle_{Q'}}{\langle Z^{-1/2}\rangle_{Q'}} \tag{2}$$

The bracket means the time-average over the MD trajectory by setting Q to the desired value and the first time derivative to 0. k_B and T are the Boltzmann constant and temperature, respectively. The weighting factor Z and the correction term G are defined as,

$$Z = \sum_i^N \frac{1}{m_i}\left(\frac{\partial Q}{\partial r_i}\right)^2 \tag{3}$$

$$G = \frac{1}{Z^2}\sum_{ij}^N \frac{1}{m_i m_j}\frac{\partial Q}{\partial r_i}\frac{\partial^2 Q}{\partial r_i \partial r_j}\frac{\partial Q}{\partial r_j} \tag{4}$$

where N means the number of the involved atoms and m denotes the atomic mass.

In the acid dissociation simulation, the coordination number (CN) of the reactive hydroxyl oxygen is chosen as

the order parameter. This approach has been successfully applied in some cases, e.g. water (Sprik, 2000) and pentaoxyphosphoranes (Davies et al., 2002; Doltsinis and Sprik, 2003).

In the simulations, the CN of the reactive oxygen (O^*) runs over all hydrogen in the system:

$$n_{\mathrm{H}} = \sum_{i=1}^{N_{\mathrm{H}}} S(|r_{\mathrm{H}_i} - r_{\mathrm{O}^*}|) \tag{5}$$

The function ($S(r)$) of CN is used to weight the contributions of the solvent particle with some suitable distance dependent function. Following Sprik (1998, 2000), we employ the Fermi function,

$$S(r) = \frac{1}{\exp[\kappa(r - r_{\mathrm{c}})] + 1} \tag{6}$$

where κ and r_{c} denote the inversion of the width and the cutoff. The particles outside the interval of $r_{\mathrm{c}} - \kappa < r < r_{\mathrm{c}} + \kappa$ are effectively counted as full or nothing.

In practice, the proper parameters can be chose from the radial distribution function (RDF) in the reactant state. In this study we use 0.10 and 1.35 Å for the width and the cutoff, respectively.

2.3. p*K*a calculation

For an acid dissociation reaction with a free-energy change ΔF, the pKa can be calculated with the thermodynamic relation,

$$\mathrm{p}K\mathrm{a} = \frac{\Delta F}{k_{\mathrm{B}} T \ln(10)} \tag{7}$$

With the aim of eliminating the finite size effects in simulations, Davies et al. (2002) designed an alternative approach to derive pKa, which is based on the relation between the radial distribution function (RDF) and the relative free energies (Chandler, 1987),

$$\mathrm{RDF}(r) = \exp\left(-\frac{\Delta F(r)}{k_{\mathrm{B}} T}\right) \tag{8}$$

So for the finite system, the probability to find the proton within the radius R_{c} from the donor oxygen reads,

$$P(R_{\mathrm{c}}) = \frac{\int_0^{R_{\mathrm{c}}} 4\pi r^2 \exp\left(-\frac{\Delta F}{k_{\mathrm{B}} T}\right) dr}{\int_0^{R_{\mathrm{max}}} 4\pi r^2 \exp\left(-\frac{\Delta F}{k_{\mathrm{B}} T}\right) dr} \tag{9}$$

Here R_{max} is the maximum O–H distance for which the free energy is calculated.By introducing the dissociation fraction as $\alpha(R_{\mathrm{c}}) = 1 - P(R_{\mathrm{c}})$, the p$K$a can be written as,

$$\mathrm{p}K\mathrm{a} = -\log\left(\frac{\alpha(R_{\mathrm{c}})^2}{P(R_{\mathrm{c}}) c_0 V}\right) \tag{10}$$

where c_0 and V denote the standard concentration and the volume, respectively.

Obviously, the calculated pKa depends on the bonding radius R_{c}. Here we use 1.22 Å by following the previous studies where it is shown that with this cutoff the acidity of 14 is reproduced for the liquid water (Davies et al., 2002).

3. RESULTS AND DISCUSSIONS

3.1. Reactant states

Figs. 1 and 2 show the results derived from the unconstrained simulations of reactant states. On Fig. 1, it is clear that the first sharp RDF peaks denote the covalent OH bonds. During the simulations, Si–O and Al–O distances are around 1.64 and 1.93 Å (marked on Fig. 2), consistent with the previous studies (Kubicki et al., 1995; Ikeda et al., 2003, 2006; Amira et al., 2006; Bylaska et al., 2007; Gomes et al., 2008; Hay and Myneni, 2008). On Fig. 1A, the second RDF peak around 1.9 Å denotes the hydrogen from the proton donating water (green lines on Fig. 2A), which amounts to 1.2 on the CN curve. That means in the solvation structure of silicic acid, the oxygen of the OH ligand has an incomplete tetrahedral configuration. The third peak around 3.1 Å includes the contributions of the other three OH ligands, the proton donating and the proton accepting water molecules, as marked in black on Fig. 2A. On Fig. 2B, one can see the leaflike solvation structures of $Al(H_2O)_6^{3+}$ where the second-shell water forms acceptor H-bonds from the first-shell waters (Bylaska et al., 2007). Thus on Fig. 1B, it is clear that the second peak denotes the hydrogen from both the second-shell

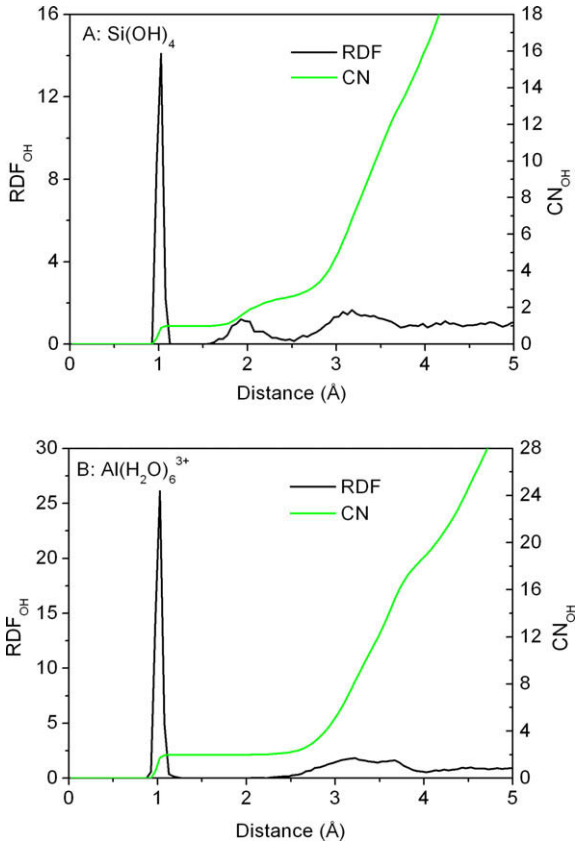

Fig. 1. RDFs and CNs of hydrogen around the oxygen of the dissociating OHs of the reactant states, derived from unconstrained simulations.

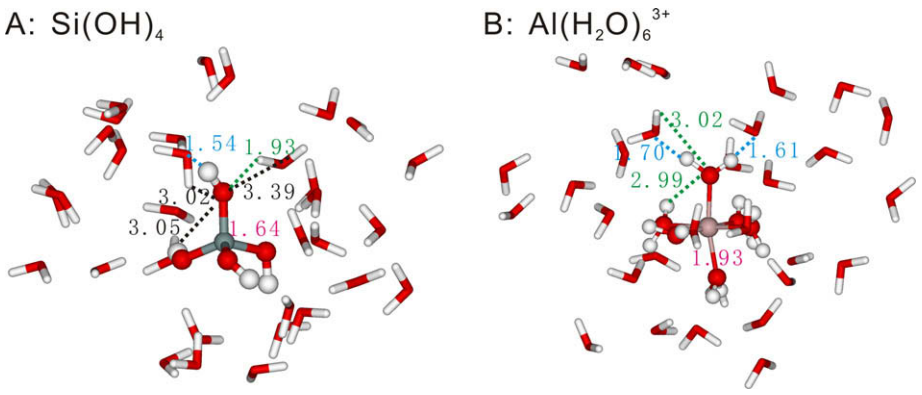

Fig. 2. Snapshots of the reactant states sampled from the unconstrained MD simulations. Cyan numbers: ion-oxygen bond-lengths; Blue numbers: H-bonds where the ligands serve as proton donors; Green numbers: the H-bonds contributing to the second RDF peaks on Fig. 1A and B; Black numbers: the H-bonds contributing to the third RDF peak shown on Fig. 1A. O: red, H: white, Si: grey and Al: faded pink. $Si(OH)_4$ and $Al(H_2O)_6^{3+}$ are shown with ball-stick models and the solvents are represented with sticks. (For interpretation of the references to color in this figure legend, the reader is referred to the web version of this paper.)

waters and the other first-shell waters (green lines on Fig. 2B).

3.2. Mean force, free energy and p*K*a

The mean force curves and integrated free-energy profiles are illustrated on Fig. 3, where the coordination number is gradually decreased to transfer the proton from the reactive oxygen to the acceptor water. On both figures, it is clear that the initial elongation gives rise to a substantial increase of the constraint force and the maxima are reached around the CN values of 0.94 and 1.9, corresponding to the OH bond-lengths of 1.12 and 1.08 Å, respectively. Subsequently, the forces gradually decrease and reach the minima at 0.4 and 1.2, respectively. The two proton transfer processes terminate at the CNs of 0.03 and 1.01, with corresponding free energy values of 15.0 and 7.7 kcal/mol, respectively. These free-energy changes yield p*K*a values of 10.9 and 5.7 according to Eq. (7). Fig. 4 shows the p*K*a curves calculated with the RDF method and Table 1 collects the comparison between experiments and these calculations. The calculations overestimate the p*K*as by 1–2 units. A similar discrepancy was observed for the calculated pKa of water using a similar computational setup (Sprik, 2000), and our results should be considered as significant. We notice that in a simulation study on Al-aqua (Ikeda et al., 2006) where Al–H coordination was taken as the reaction coordinate for OH dissociation and HCTH functional was used (Hamprecht et al., 1998), the authors obtained $\Delta F = 8.0$ kcal/mol (p*K*a = 5.8) by sampling only 4 points, which should be considered very fortuitous.

There are various factors that contribute to a limited accuracy of the calculated free energy: the obvious approximate nature of the DFT functional employed to calculate the interactions and the small size of the periodic box. The factors in DFT are difficult to circumvent, e.g. BLYP functional underestimates the H-bonding energy by 1 kcal/mol (Sprik et al., 1996), but in principle the finite size effect can be improved systematically by performing extended simulations (Frenkel and Smit, 2002). So with the assumption that CN is an optimal reaction coordinate, the pristine technique actually can make estimates as well as DFT allows.

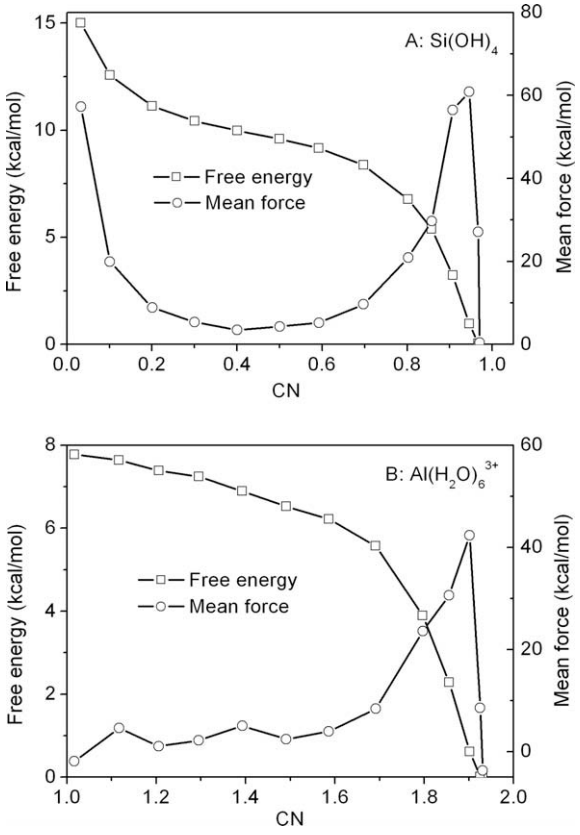

Fig. 3. Mean force curves and integrated free-energy profiles as functions of coordination numbers. For the free energies, the equilibrium CN values of 0.96 and 1.95 are taken as the reference points of the two systems, respectively. The curves are used to guide eyes.

In the RDF method, some more errors can be introduced. (1) Since the idea behind is the RDF-free energy

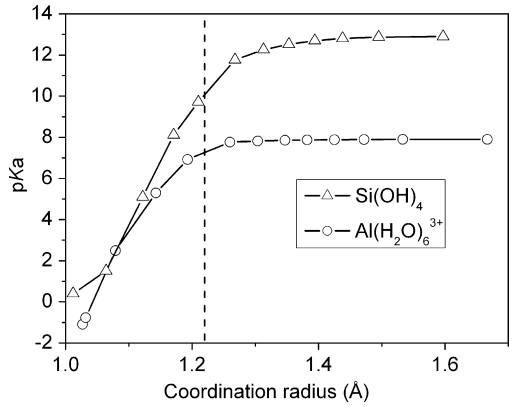

Fig. 4. p*K*a values calculated with Eq. (10).

Table 1
Experimental and calculated p*K*a values.

p*K*a	$Si(OH)_4$	$Al(H_2O)_6^{3+}$
Exp.	9.8[a]	5.5[b]
Eq. (7)	10.9	5.6
Eq. (10)	10.0	7.2

[a] Iler, 1979.
[b] Martin, 1988.

relation, it should be precise enough for the distance constraint, which controls the distance between two particles (Meijer and Sprik, 1998). However, in coordination constrained simulations, the constraint force also acts on the other protons besides the leaving one. When transforming the CN values to the distances (as done in Eq. (9) and Fig. 4), the effect is actually equivalent to assigning the work done on all protons to the leaving one. This should be especially obvious when the protons of the other solvent waters (except the acceptor) get close enough to attack the newly-created conjugate base because at that moment a considerable part of constraint force works on those protons. (2) From the plots in Fig. 4, it is clear that the final result is very sensitive to the selected bonding radius. Because the used distance criterion is picked up from the dissociation curve of BLYP water (Sprik, 2000), the transferability is obviously questionable, for different systems and different functionals. These additional factors render the final results unreliable. On the basis of the above comparisons and analyses, the pristine way should be favored, which shows an error margin of 1 p*K*a unit for the two species.

3.3. Approximate transition states and product states

On the two mean force curves, the points of 0.4 and 1.2 represent nearly vanished forces, which are thus in the closet of the transition states (Sprik, 2000). Here one should be aware that because the chemical reactions are normally dominated by several reaction coordinates which need to be taken into account when locating the exact reaction pathways, the configurations obtained here only yield the approximate transition states. Fig. 5 shows that at these stages, the hydronium ions have formed and constitute contact ion pairs with the newly-created conjugated bases where the breaking OH bonds are stretched to about 1.45 Å. The hydroniums are H-bonded with two water molecules and represent a structure similar to the Eigen cation as shown in Fig. 6A (Marx et al., 1999) (marked on Fig. 5). During the simulations, it is observed that the protons in the complexes diffuse to the nearest water occasionally, but they come back very quickly.

As the coordination numbers are decreased further to 0.03 and 1.01 for the two systems respectively, the protons attached on the water become free to initiate the Grotthuss-type diffusion (Marx et al., 1999). After the proton transfer complete, the Si–O and Al–O bonds shrink to 1.60 and 1.86 Å, respectively (Fig. 6). At the same time, the solvation structures have changed: for silicic anion, three water molecules are H-bonded to the dangling oxygen atom; for $Al(H_2O)_5OH^{2+}$, two water molecules donate H-bonds to

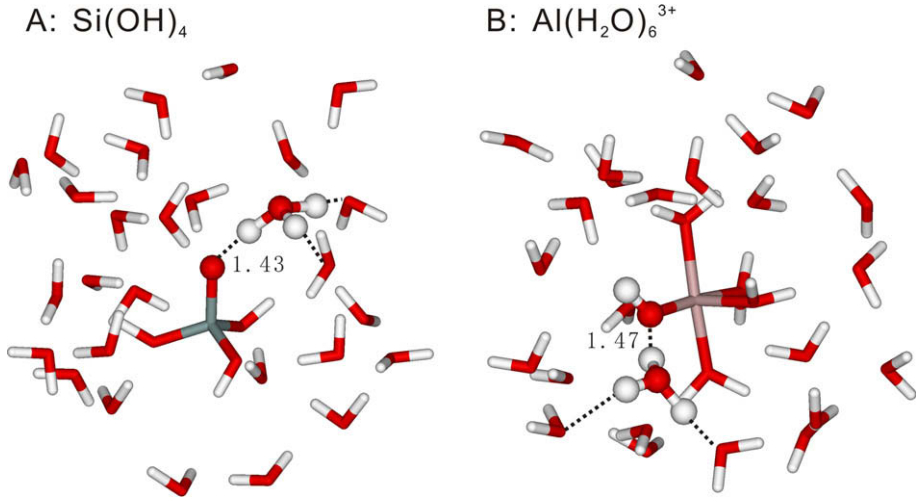

Fig. 5. Snapshots illustrating the contact ion pairs which are close to the transition states. O: red, H: white, Si: grey and Al: faded pink. (For interpretation of the references to color in this figure legend, the reader is referred to the web version of this paper.)

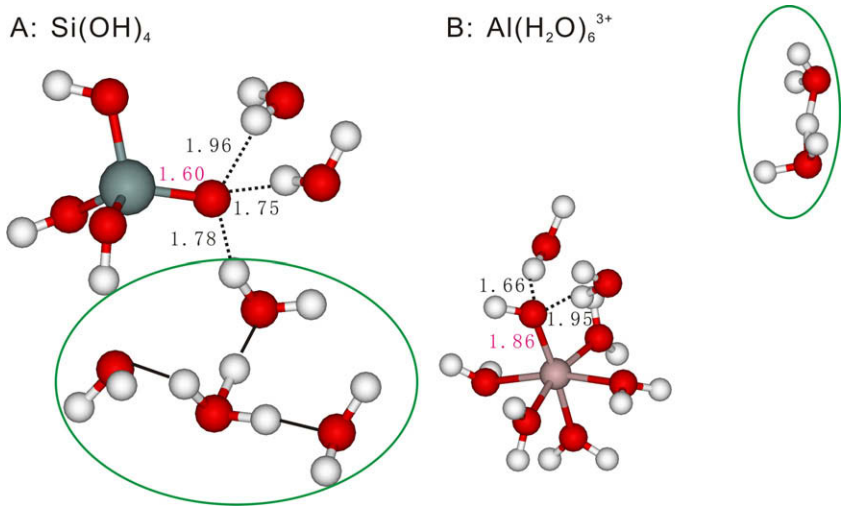

Fig. 6. Snapshots sampled from the product states. The green circles denote the Eigen cation ($H_9O_4^+$) and the Zundel cation ($H_5O_2^+$). The ion-oxygen bond-lengths are shown in cyan and the H-bond distances are in black. The other water molecules are removed for clarity. O: red, H: white, Si: grey and Al: faded pink. (For interpretation of the references to color in this figure legend, the reader is referred to the web version of this paper.)

the newly created OH ligand. When proton enters the aqueous solution, two typical solvation structures can be observed, i.e. the Eigen cation ($H_9O_4^+$) and the Zundel cation ($H_5O_2^+$) as pictured in Fig. 6. The former has a hydrated-hydronium structure and the latter is a proton-shared complex and it has been shown that both complexes exist during the proton transfer processes (Marx et al., 1999; Marx, 2006).

4. SUMMARY

In this study, first-principles molecular dynamics simulations are employed to explore the hydroxyl dissociation mechanisms of silicic acid and the hexa-aqua of Al^{3+}. The solvated systems are treated with full quantum mechanical techniques by taking account of the solvents explicitly. The dissociation reactions are enforced with the method of coordination constraint and the free-energy profiles are calculated with the thermodynamic integration.

By tracing the dissociation processes, the reactant, product and approximate transition states are characterized. In the reactant states, the equilibrium Si–O and Al–O bond-lengths are about 1.64 and 1.93 Å and after deprotonation, they shrink to 1.60 and 1.86 Å, respectively. The transition states show the configurations of contact ion pair with the breaking OH bonds stretched to around 1.45 Å. The free-energy changes are found about 15.0 and 7.7 kcal/mol for silicic acid and Al-aqua, respectively.

Based on the simulation results, the first p*K*as are derived in both the pristine thermodynamic and the RDF ways. By analyzing the error origins, the latter method can include more artifacts and uncertainties and thus, we suggest that the pristine way should be favored, which represents an error margin of 1 p*K*a. These calibration tests prove that the present methodology can provide accurate p*K*a values for these geochemically important clusters and therefore, it should be reliable to apply this technique to predict the acidities of the groups which have more complex chemical environments, such as hydroxyls on mineral surfaces and bio-ligands complexed with metal cations.

ACKNOWLEDGMENT

We acknowledge National Science Foundation of China (No. 40373024) and the support (No. 2008-II-14) from the State Key Laboratory for Mineral Deposits Research, Nanjing University. We thank Dr. James Kubicki, Dr. Frank Podosek and anonymous reviewers for their generous helps on improving the paper.

REFERENCES

Amira S., Spangberg D. and Hermansson K. (2006) OD vibrations and hydration structure in an Al^{3+}(aq) solution from a Car–Parrinello molecular-dynamics simulation. *J. Chem. Phys.* **124**, 104501.

Becke A. D. (1988) Density-functional exchange-energy approximation with correct asymptotic-behavior. *Phys. Rev. A* **38**, 3098–3100.

Bickmore B. R., Rosso K. M., Nagy K. L., Cygan R. T. and Tadanier C. J. (2003) Ab initio determination of edge surface structures for dioctahedral 2:1 phyllosilicates: implications for acid–base reactivity. *Clays Clay Miner.* **51**, 359–371.

Bickmore B. R., Rosso K. M., Tadanier C. J., Bylaska E. J. and Doud D. (2006) Bond–valence methods for pK(a) prediction. II. Bond-valence, electrostatic, molecular geometry, and solvation effects. *Geochim. Cosmochim. Acta* **70**, 4057–4071.

Bickmore B. R., Tadanier C. J., Rosso K. M., Monn W. D. and Eggett D. L. (2004) Bond–valence methods for pK(a) prediction: critical reanalysis and a new approach. *Geochim. Cosmochim. Acta* **68**, 2025–2042.

Bylaska E. J., Valiev M., Rustad J. R. and Weare J. H. (2007) Structure and dynamics of the hydration shells of the Al^{3+} ion. *J. Chem. Phys.* **126**, 104505.

Car R. and Parrinello M. (1985) Unified approach for molecular-dynamics and density-functional theory. *Phys. Rev. Lett.* **55**, 2471–2474.

Carter E. A., Ciccotti G., Hynes J. T. and Kapral R. (1989) Constrained reaction coordinate dynamics for the simulation of rare events. *Chem. Phys. Lett.* **156**, 472–477.

Casey W. H. and Rustad J. R. (2007) Reaction dynamics, molecular clusters, and aqueous geochemistry. *Annu. Rev. Earth Planet. Sci.* **35**, 21–46.

Casey W. H., Rustad J. R. and Spiccia L. (2009) Minerals as molecules-use of aqueous oxide and hydroxide clusters to understand geochemical reactions. *Chem. A Eur. J.* **15**, 4496–4515.

Chandler D. (1987) *Introduction to Modern Statistical Mechanics*. Oxford, University Press, Oxford.

Churakov S. V. (2006) Ab initio study of sorption on pyrophyllite: structure and acidity of the edge sites. *J. Phys. Chem. B* **110**, 4135–4146.

Churakov S. V. (2007) Structure and dynamics of the water films confined between edges of pyrophyllite: a first principle study. *Geochim. Cosmochim. Acta* **71**, 1130–1144.

Davies J. E., Doltsinis N. L., Kirby A. J., Roussev C. D. and Sprik M. (2002) Estimating pK(a) values for pentaoxyphosphoranes. *J. Am. Chem. Soc.* **124**, 6594–6599.

Doltsinis N. L. and Sprik M. (2003) Theoretical pK(a) estimates for solvated P(OH)(5) from coordination constrained Car–Parrinello molecular dynamics. *Phys. Chem. Chem. Phys.* **5**, 2612–2618.

Frenkel D. and Smit B. (2002) *Understanding Molecular Simulation*, second ed. Academic Press, San Diego, CA.

Gomes J. R. B., Cordeiro M. N. D. S. and Jorge M. (2008) Gas-phase molecular structure and energetics of anionic silicates. *Geochim. Cosmochim. Acta* **72**, 4421–4439.

Hamprecht F. A., Cohen A. J., Tozer D. J. and Handy N. C. (1998) Development and assessment of new exchange-correlation functionals. *J. Chem. Phys.* **109**, 6264–6271.

Hay M. B. and Myneni S. C. B. (2008) Geometric and electronic structure of the aqueous Al(H2O)(6)(3+) complex. *J. Phys. Chem. A* **112**, 10595–10603.

Ikeda T., Hirata M. and Kimura T. (2003) Ab initio molecular dynamics study of polarization effects on ionic hydration in aqueous $AlCl_3$ solution. *J. Chem. Phys.* **119**, 12386.

Ikeda T., Hirata M. and Kimura T. (2006) Hydrolysis of Al^{3+} from constrained molecular dynamics. *J. Chem. Phys.* **7**, 074503.

Iler R. K. (1979) *The Chemistry of Silica*. John Wiley & Sons, New York.

Kleinman L. and Bylander D. M. (1982) Efficacious form for model pseudopotentials. *Phys. Rev. Lett.* **48**, 1425–1428.

Kubicki J. D. (2001) Self-consistent reaction field calculations of aqueous Al^{3+}, Fe^{3+}, and Si^{4+}: calculated aqueous-phase deprotonation energies correlated with experimental ln(*K*a) and p*K*a. *J. Phys. Chem. A* **105**, 8756–8762.

Kubicki J. D., Apitz S. E. and Blake G. A. (1995) G2 theory calculations on [H3SiO4](−), [H4SiO4], [H3AlO4](2−), [H4AlO4](−) and [H5AlO4]: basis set and electron correlation effects on molecular structures, atomic charges, infrared spectra, and potential energies. *Phys. Chem. Miner.* **22**, 481–488.

Laasonen K., Sprik M., Parrinello M. and Car R. (1993) Ab-initio liquid water. *J. Chem. Phys.* **99**, 9080–9089.

Lee C., Yang W. and Parr R. G. (1988) Development of the colle-salvetti correlation-energy formula into a functional of the electron-density. *Phys. Rev. B* **37**, 785–789.

Liu X. D., Lu X. C., Wang R. C., Zhou H. Q. and Xu S. J. (2008) Surface complexes of acetate on edge surfaces of 2:1 type phyllosilicate: insights from density functional theory calculation. *Geochim. Cosmochim. Acta* **72**, 5896–5907.

Martin R. B. (1988) Bioinorganic chemistry of aluminum. *Met. Ions Biol. Syst.* **24**, 1–57.

Martin R. B. (1991) Fe^{3+} and Al^{3+} hydrolysis equilibria-cooperativity in Al^{3+} hydrolysis reactions. *J. Inorg. Biochem.* **44**, 141–147.

Marx D. (2006) Proton transfer 200 years after von Grotthuss: insights from ab initio simulations. *ChemPhysChem* **7**, 1848–1870.

Marx D., Tuckerman M. E., Hutter J. and Parrinello M. (1999) The nature of the hydrated excess proton in water. *Nature* **397**, 601–604.

Meijer E. J. and Sprik M. (1998) Ab initio molecular dynamics study of the reaction of water with formaldehyde in sulfuric acid solution. *J. Am. Chem. Soc.* **120**, 6345–6355.

Rustad J. R., Dixon D. A., Kubicki J. D. and Felmy A. R. (2000a) Gas-phase acidities of tetrahedral oxyacids from ab initio electronic structure theory. *J. Phys. Chem. A* **104**, 4051–4057.

Rustad J. R., Dixon D. A. and Felmy A. R. (2000b) Intrinsic acidity of aluminum, chromium (III) and iron (III) mu(3)-hydroxo functional groups from ab initio electronic structure calculations. *Geochim. Cosmochim. Acta* **64**, 1675–1680.

Rustad J. R., Dzwinel W. and Yuen D. A. (2001) Computational approaches to nanomineralogy. Nanoparticles and the environment. *Rev. Mineral. Geochem.* **44**, 191–216.

Rustad J. R., Wasserman E. and Felmy A. R. (1999) Molecular modeling of the surface charging of hematite – II. Optimal proton distribution and simulation of surface charge versus pH relationships. *Surf. Sci.* **424**, 28–35.

Sefcik J. and Goddard W. A. (2001) Thermochemistry of silicic acid deprotonation: comparison of gas-phase and solvated DFT calculations to experiment. *Geochim. Cosmochim. Acta* **65**, 4435–4443.

Sigel H. and Sigel A. (1988) *Aluminum and its Role in Biology (Metal Ions Biol. Systems 24)*. Marcel Dekker, New York.

Sprik M. (1998) Coordination numbers as reaction coordinates in constrained molecular dynamics. *Faraday Discuss.* **110**, 437–445.

Sprik M. (2000) Computation of the pK of liquid water using coordination constraints. *Chem. Phys.* **258**, 139–150.

Sprik M. and Ciccotti G. (1998) Free energy from constrained molecular dynamics. *J. Chem. Phys.* **109**, 7737–7744.

Sprik M., Hutter J. and Parrinello M. (1996) Ab initio molecular dynamics simulation of liquid water: comparison three gradient-corrected density functionals. *J. Chem. Phys.* **105**, 1142–1152.

StÖber W. (1967) Formation of silicic acid in aqueous suspensions of different silica modifications. In *Equilibrium concepts in natural water systems. Advances in Chemistry Series, Am. Chem. Soc.* **67,** 61–182.

Trinh T. T., Jansen A. P. J., van Santen R. A. and Meijer E. J. (2009). *J. Phys. Chem. C* **113**, 2647–2652.

Troullier N. and Martins J. L. (1991) Efficient pseudopotentials for plane-wave calculations. *Phys. Rev. B* **43**, 1993–2006.

van Erp T. S. and Meijer E. J. (2004) Proton-assisted ethylene hydration in aqueous solution. *Angew. Chem., Int. Ed.* **43**, 1659–1662.

Yokel R. A. (2004) In *Elements and their Compounds in the Environment: Occurrence, Analysis, and Biological Relevance*, second ed., vol. 2 (eds. E. Merian, M. Anka, M. Ihnat and M. Stoeppler). Wiley, New York. pp. 635–658.

Associate editor: James Kubicki